University of South Carolina
Scholar Commons

Faculty Publications | Chemical Engineering, Department of

7-13-2015

Optimum 3D Matrix Stiffness for Maintenance of Cancer Stem Cells Is Dependent on Tissue Origin of Cancer Cells

Esmaiel Jabbari

Samaneh K. Sarvestani

Leily Daneshian

Seyedsina Moeinzadeh

Follow this and additional works at: https://scholarcommons.sc.edu/eche_facpub

 Part of the Chemical Engineering Commons

PLOS | ONE

RESEARCH ARTICLE

Optimum 3D Matrix Stiffness for Maintenance of Cancer Stem Cells Is Dependent on Tissue Origin of Cancer Cells

Esmaiel Jabbari[1]*, Samaneh K. Sarvestani[1], Leily Daneshian[1], Seyedsina Moeinzadeh[1]

Biomimetic Materials and Tissue Engineering Laboratory, Department of Chemical Engineering, University of South Carolina, Columbia, SC, 29208, United States of America

* jabbari@mailbox.sc.edu

CrossMark
click for updates

OPEN ACCESS

Citation: Jabbari E, Sarvestani SK, Daneshian L, Moeinzadeh S (2015) Optimum 3D Matrix Stiffness for Maintenance of Cancer Stem Cells Is Dependent on Tissue Origin of Cancer Cells. PLoS ONE 10(7): e0132377. doi:10.1371/journal.pone.0132377

Editor: Adam J. Engler, University of California, San Diego, UNITED STATES

Received: March 2, 2015

Accepted: June 13, 2015

Published: July 13, 2015

Copyright: © 2015 Jabbari et al. This is an open access article distributed under the terms of the Creative Commons Attribution License, which permits unrestricted use, distribution, and reproduction in any medium, provided the original author and source are credited.

Data Availability Statement: All relevant data are within the paper.

Funding: This work was supported by research grants to EJ from the National Science Foundation under grant No. CBET1403545 and the National Institutes of Health under grant No. AR063745. The funding agencies did not have any role in designing experiments or in preparation of this manuscript.

Competing Interests: The authors indicate no potential conflicts of interest.

Abstract

Introduction

The growth and expression of cancer stem cells (CSCs) depend on many factors in the tumor microenvironment. The objective of this work was to investigate the effect of cancer cells' tissue origin on the optimum matrix stiffness for CSC growth and marker expression in a model polyethylene glycol diacrylate (PEGDA) hydrogel without the interference of other factors in the microenvironment.

Methods

Human MCF7 and MDA-MB-231 breast carcinoma, HCT116 colorectal and AGS gastric carcinoma, and U2OS osteosarcoma cells were used. The cells were encapsulated in PEGDA gels with compressive moduli in the 2-70 kPa range and optimized cell seeding density of $0.6x10^6$ cells/mL. Micropatterning was used to optimize the growth of encapsulated cells with respect to average tumorsphere size. The CSC sub-population of the encapsulated cells was characterized by cell number, tumorsphere size and number density, and mRNA expression of CSC markers.

Results

The optimum matrix stiffness for growth and marker expression of CSC sub-population of cancer cells was 5 kPa for breast MCF7 and MDA231, 25 kPa for colorectal HCT116 and gastric AGS, and 50 kPa for bone U2OS cells. Conjugation of a CD44 binding peptide to the gel stopped tumorsphere formation by cancer cells from different tissue origin. The expression of YAP/TAZ transcription factors by the encapsulated cancer cells was highest at the optimum stiffness indicating a link between the Hippo transducers and CSC growth. The optimum average tumorsphere size for CSC growth and marker expression was 50 μm.

Conclusion

The marker expression results suggest that the CSC sub-population of cancer cells resides within a niche with optimum stiffness which depends on the cancer cells' tissue origin.

Introduction

A major factor contributing to cancer mortality is relapse after surgery, radiation or drug therapy [1,2]. Breast cancer recurrence affects 30% of the patients [3] while up to 50% of colorectal cancer patients experience relapse [4]. Malignancy in cancer is believed to be related to the existence of a small sub-population of stem cells (CSCs) in the tumor with elevated resistance to cancer therapy [5]. Consistent with that, the most aggressive triple-negative breast cancer or metastatic stage III colon cancer has the highest sub-population of CSCs among different types [6,7]. Therefore, understanding factors in the tumor microenvironment that contribute to CSC growth is central to cancer treatment [8].

Substrate rigidity affects lineage commitment and fate of stem cells [9]. A soft substrate directs differentiation of mesenchymal stem cells (MSCs) to neurogenic lineage whereas a substrate with intermediate and high stiffness leads to the differentiation of MSCs to myogenic and osteogenic lineages, respectively [10]. Substrate rigidity also affects the fate of malignant cells [11] as the rigidity of hyperplastic ERbB2 over-expressing MCF10AT human breast epithelial cells increased in response to higher stiffness of the collagen matrix [12]. The role of 3D matrix stiffness on growth and marker expression of CSC sub-population of cancer cells from different cell lines has not been investigated and the relation between matrix stiffness, CSC growth, and epithelial to mesenchymal transition (EMT) is not known.

Since the process of cancer initiation can take a long time and it is difficult to study in vivo, in vitro culture systems have been developed to study CSCs. CSCs grown in suspension on a non-adherent substrate are morphologically different compared to those in the tumor tissue [13]. Natural ECM components are widely used as a 3D matrix to promote in vivo like morphogenesis of CSCs [14] but biological matrices are inherently variable in composition and variations in matrix composition can alter ligand/receptor density [11]. Further, ligand-receptor interactions and chemical stimuli in biologic matrices often mask the effect of mechanical stimuli on cells [15]. We previously demonstrated that breast CSCs selectively grow in non-adherent polyethylene glycol diacrylate (PEGDA) gels and form tumorspheres when cancer cells are encapsulated in the gel [16,17]. Due to the absence of ligand-receptor interaction, the non-stem cell population of the encapsulated cells did not grow in the gel which led to selective enrichment of CSCs. We previously observed a biphasic relation between the expression of CSC markers and matrix stiffness for breast cancer cells [16]. The change in tissue stiffness with cancer progression could be an intrinsic response by the CSC sub-population to optimize growth and expression of stem cell markers. Human HCT8 colorectal carcinoma cells exhibited a metastatic phenotype in the 20–50 kPa stiffness range [18] whereas osteosarcoma cells interacted optimally with substrates at 55 kPa stiffness [19]. We hypothesized that the optimum matrix stiffness for growth and expression of CSC markers depended on the cancer cells' tissue origin. Therefore, the objective of this work was to investigate the effect of gel stiffness on growth and marker expression of CSC sub-population of cancer cells derived from different tissues. The tested cancer cells were MCF7 and MDA-MB-231 breast adenocarcinoma, HCT116 colorectal carcinoma, AGS gastric adenocarcinoma, and U2OS osteosarcoma human cell lines

with non-tumorigenic MCF10A epithelial cell line used as the control. Micropatterning was used to control the average size of the CSC colonies formed by the cancer cells in PEGDA gel.

Materials and Methods

Materials

Linear polyethylene glycol (PEG) with molecular weight (MW) of 3.4 kDa was purchased from Acros (Pittsburg, PA). 4-(2-hydroxyethoxy)phenyl-(2-hydroxy-2-propyl) ketone (Irgacure-2959) photoinitiator was from CIBA (Tarrytown, NY). Acryloyl chloride (Ac) and calcium hydride were from Sigma-Aldrich (St. Louis, MO). The protected amino acids and Rink Amide NovaGel resin were received from EMD Biosciences (San Diego, CA). Piperidine, tetrahydrofuran (THF), trimethylsilane (TMS), triethylamine (TEA), acrylic acid, dimethylsulfoxide (DMSO), and ethylenediaminetetraacetic acid disodium salt (EDTA) were from Sigma-Aldrich. N,N-dimethylformamide (DMF), acetonitrile (MeCN), N,N-diisopropylethylamine (DIEA), N,N'-diisopropylcarbodiimide (DIC), triisopropylsilane (TIPS), N,N-dimethylaminopyridine (DMAP), hydroxybenzotriazole (HOBt), dichloromethane (DCM), and trifluoroacetic acid (TFA) were received from Acros. Spectro/Por dialysis tube (MW cutoff 3.5 kDa) was from Spectrum Laboratories (Rancho Dominquez, CA).

MCF7 (HTB-22) breast adenocarcinoma, MDA-MB-231 (HTB-26, hereafter denoted by MDA231) breast adenocarcinoma, HCT116 (CCL-247) colorectal carcinoma, AGS (CRL-1739) gastric adenocarcinoma, U2OS (HTB-96) osteosarcoma cell lines, and MCF10A (CRL-10317) non-tumorigenic epithelial cells were purchased from ATCC (Manassas, VA). Phosphate-buffer saline (PBS) and Dulbecco's Modified Eagle's Medium (DMEM) were received from GIBCO BRL (Grand Island, NY). Horse serum and DMEM-F12 medium were from PAA Laboratories (Etobicoke, Ontario) and MediaTech (Manassas, VA), respectively. Trypsin-EDTA, RPMI-160 cell culture medium, fetal bovine serum (FBS), Alexa Fluor 594 Phalloidin, and Quant-it PicoGreen dsDNA reagent kit were from Invitrogen (Carlsbad, CA). Basic fibroblast growth factor (bFGF) and epidermal growth factor (EGF) were from Lonza (Allendale, NJ). Bovine serum albumin (BSA) was from Jackson ImmunoResearch (West Grove, PA). Alexa Fluor Phalloidin, CellTracker red CMTPX dye, and Live/Dead cell viability kit were from Molecular Probes (Life Technologies, Grand Island, NY). Paraformaldehyde, 4,6-diamidino-2-phenylindole (DAPI), insulin, hydrocortisone, cholera toxin, penicillin, and streptomycin were received from Sigma-Aldrich. Monoclonal rabbit antibody against YAP/TAZ transcription factors was received from Cell Signaling (Danvers, MA).

Macromer and peptide synthesis

The hydroxyl end-groups of the PEG macromer was reacted with acryloyl chloride to produce PEG diacrylate (PEGDA), as we described previously [16,17]. The product was purified by precipitation in cold ethyl ether twice, dialyzed against deionized (DI) water from DMSO, and freeze-dried. The chemical structure of the functionalized macromer was characterized by ^{1}H-NMR as we described previously [16]. The acrylamide-terminated CD44 binding peptide Ac-RLVSYNGIIFFLK was synthesized manually on Rink Amide resin in the solid phase using a previously described procedure [20]. After cleavage from the resin, the Ac-terminated peptide was purified by preparative HPLC, lyophilized, and the product was characterized with an Electro Spray Ionization (ESI) spectrometer as we described previously [20]. A similar procedure was used to synthesize the scrambled (mutant) Ac-VLFGFLKIYSRIN peptide.

Cultivation of tumor cells

The following procedure was used to encapsulate tumor cells in the PEGDA gel [16]. MDA231, MCF7, HCT116, and AGS tumor cells were cultured on adherent tissue culture plates in RMPI-1640 medium with 10% FBS under 5% CO_2 whereas U2OS cells were cultivated in DMEM medium according to supplier's instructions. MCF10A cells were cultured in DMEM-F12 medium supplemented with 0.5 mg/mL Hydrocortisone, 10 μg/mL insulin, 100 ng/mL Cholera toxin, 20 ng/mL EGF and, 5% horse serum according to supplier's instructions. The 2D cell cultures were trypsinized after reaching 70% confluency and re-suspended in PBS at a density of $1x10^7$ cells/mL. The gel precursor solution was prepared by dissolving 100 mg PEGDA macromer in the photoinitiator solution (10 mg Irgacure-2959 in 1 mL PBS) and the solution was sterilized by filtration. Next, a specified volume of the tumor cells was uniformly suspended in the gel precursor solution by gentle mixing to a final density of 0.3–$2.0x10^6$ cells/mL. The cell-suspended gel precursor solution was crosslinked by UV irradiation with a UV lamp (Black-Ray, UVP, Upland, CA) at peak wavelength of 365 nm as we described previously [16]. The compressive modulus of the cell-encapsulated gels was measured with a rheometer (TA Instruments, New Castle, DE) under a uniaxial compressive force as we previously described [16]. Precursor solutions with 5, 10, 15, 20, and 25 wt% PEGDA macromer produced cell-encapsulated gels with 2, 5, 25, 50, and 70 kPa compressive moduli, respectively [16]. After crosslinking, the gels were cut into disks and incubated in the stem cell medium to form tumorspheres. The stem cell medium consisted of DMEM-F12 supplemented with 0.4% BSA, 5 mg/mL insulin, 40 ng/mL bFGF, 20 ng/mL EGF, 5% horse serum, 100 U/mL penicillin, and 100 mg/mL streptomycin [21].

Micropatterning

The following procedure was used to encapsulate cancer cells in a micropatterned gel. To physically separate the cell-encapsulated gel layer from the rigid glass substrate, 40 μL of the gel precursor solution (25 wt% PEGDA without cells) was transferred to a glass slide with the edges covered with a biomedical-grade adhesive tape to control gel thickness to within 100 μm. Next, the assembly was covered with a glass cover slip and UV irradiated for 8 min. To generate a pattern, UV masks were designed with an AutoCAD software (AutoCAD 2010, Autodesk, San Rafael, CA) and printed on a transparent sheet as described [22]. The glass edges were covered with a second layer of adhesive tape and 40 μL of the cell-suspended gel precursor solution was transferred to the gel-covered glass slide, the UV mask was placed over the solution and pressed against the adhesive tape with a glass slide, and UV irradiated for 5 min. After gelation the mask was removed, the cell-encapsulated gel was washed with PBS and UV irradiated for an additional 3 min to complete gelation. Next, the patterned cell-encapsulated gel was washed with PBS, peeled from the glass slide, and cultivated in the stem cell culture medium. For live cell tracking, the tumor cells were incubated with CellTracker dye (1:1000 dilution) prior to encapsulation and the stained live cells were imaged with an inverted fluorescent microscope (Nikon Eclipse Ti-ε, Melville, NY).

Tumorsphere imaging and determination of cell number

Viability of the encapsulated cells was determined two days after encapsulation with Live/Dead assay as we described previously [16]. To measure size and number of the encapsulated tumorspheres, the cell nuclei and cytoskeleton were visualized by staining with DAPI and phalloidin, respectively, and imaged with a Nikon fluorescent microscope as described previously [16,17]. Number and size distribution of the tumorspheres were quantified by dividing the images into smaller squares and counting the number of spheres and measuring their size.

Table 1. Forward and reverse sequence for the PCR primers.

PCR Primer	Forward	Reverse
human GAPDH	5'-GAGTCAACGGATTTG GTCGT-3'	5'-TTGATTTTGGAGGGATCTCG-3'
human CD44	5'-GGCTTTCAATAGCACCTTGC-3'	5'-ACACCCCTGTGTTGTTTGCT-3'
human ABCG2	5'-CACCTTATTGGCCTCAGGAA-3'	5'-CCTGCTTGGAAGGCTCTATG-3'
human CD133	5'-GCATTGGCATCTTCTATGGTT-3'	5'-CGCCTTGTCCTTGGTAGTGT-3'
Human Oct4	5'-CGCCGTATGAGTTCTGTG-3'	5'-GGTGATCCTCTTCTGCTTC-3'
human TGF-β	5'-CCGGAGGTGATTTCCATCTA-3'	5'-CTCCATTGCTGAGACGTCAA-3'
human EGFR	5'-CAGCGCTACCTTGTCATTCA-3'	5'-TGCACTCAGAGAGCTCAGGA -3'

doi:10.1371/journal.pone.0132377.t001

Double-stranded DNA content of the gels, as a measure of cell number, was measured with a Quant-it PicoGreen assay as described previously [23].

Real time PCR Analysis

At each time point, samples were manually homogenized and sonicated to rupture the membrane of encapsulated cells. Total cellular RNA of the samples was isolated using TRIzol as previously described [23]. After reverse transcription (Promega, Madison, WI), the converted cDNA was quantified by RT-qPCR with SYBR green RealMasterMix (Eppendorf, Hamburg, Germany) using Bio-Rad CXF96 PCR (Bio-Rad, Hercules, CA) and the appropriate gene specific primers. Primers were designed and selected using Primer3 web-based software as previously described [24] and synthesized by Integrated DNA technologies (Coralville, IA). The list of forward and reverse primer sequences are provided in Table 1. The designed primer sequences matched with the reported sequences for human CD44, ABCG2, CD133, OCT4, TGF-β, EGFR, and GAPDH [25–28]. The PCR data was analyzed using ΔΔct Real time analysis method as previously described [29]. mRNA expressions were normalized against GAPDH reference gene and fold changes were compared to those in the same group at time zero.

Flow cytometry

The cell-encapsulated gels were fixed with 4% paraformaldehyde, washed with PBS, and incubated in oxidative degradation solution (0.1M $CoCl_2$ in 20% hydrogen peroxide) for 2 h [30]. After gel degradation, the suspension was centrifuged and the cells were washed with cold PBS containing 5% BSA. Next, the cells were incubated with phycoerythrin (PE) mouse anti-human CD24 and fluorescein isothiocyanate (FITC) mouse anti-human CD44 (BD Biosciences, Franklin Lakes, NJ) in PBS with 5% BSA for 45 min on ice in dark. Then, the cells were washed with cold PBS with 5% BSA and analyzed by a flow cytometer (FC500, Beckman Coulter, Brea, CA).

Immunoblotting and protein analysis

Samples were homogenized in RIPA buffer and the homogenized samples were centrifuged for 5 min to isolate the total proteins. Next, the proteins were separated by standard SDS-PAGE using the Mini-gel system (Bio-Rad) and transferred to a nitrocellulose membrane by the semi-dry transfer apparatus (Bio-Rad). Membranes were incubated in the blocking buffer at ambient conditions for 1 h followed by incubation with primary antibodies (1:1000) overnight at 4°C. After washing, the membranes were incubated with horseradish peroxidase-conjugated secondary antibodies (1:5000) for 1 h at ambient conditions. After extensive washing with a mixture of tris-buffered saline and Tween-20 (TBST), the membrane was incubated with ECL

detection reagents and exposed to an X-ray film. The intensity of the bands was quantified with the Image-J software (National Institutes of Health, Bethesda, MD).

Statistical analysis

All experiments were done in triplicate and quantitative data expressed as means ± standard deviation. Significant differences between groups were evaluated using a two-way ANOVA with replication test, followed by a two-tailed Students t-test. To account for multiple pair comparisons, p-values from the t-tests were corrected using False Discovery Rate (FDR) method [31]. A value of $p < 0.05$ was considered statistically significant.

Results

Dependence of tumorsphere growth on initial cell seeding density

Effect of initial cell seeding density on tumorsphere formation was investigated with MDA231 cells at the optimum gel modulus of 5 kPa (Fig 1). The gel modulus for MDA213 cells is optimized with respect to tumorsphere formation in the following section on "Dependence of optimum matrix stiffness for CSCs on tissue origin." DAPI and Phalloidin stained image of the encapsulated cells as a function of initial cell density from $0.3x10^6$ to $2x10^6$ cells/mL are shown in Fig 1A at day zero (left column) and after 9 days incubation (right column). CD44 cell membrane glycoprotein is used as a marker for characterization of breast, colon, gastric, head and neck, liver, ovarian, pancreatic, and prostate cancers in combination with other CSC markers [5]. ABCG2 of ABC transporter proteins is a well-studied marker for breast CSCs [32] and its expression is up-regulated in MDA231 CSC sub-population [33]. EGFR expression is up-regulated in MDA231 cells [34]. MDA231 cells encapsulated in the gel at a relatively low seeding density of $0.3x10^6$ cells/mL remained as single cells after 9 days without a significant increase in cell number (Fig 1B) or CSC marker expression (Fig 1C–1E). The encapsulated cells at high densities of $1.5x10^6$ and $2x10^6$ cells/mL showed cell aggregation (fourth and fifth rows in Fig 1A) and a significant increase in cell number after 9 days (Fig 1B) but the encapsulated cells did not form tumorspheres as the expression of CSC markers did not increase (Fig 1C–1E). Conversely, the encapsulated cells at moderate densities of $0.6x10^6$ and $1x10^6$ cells/mL formed tumorspheres (second and third rows in Fig 1A) with a significant increase in cell number (Fig 1B) and expression of CSC markers (Fig 1C–1E, statistically higher than the groups with initial cell density of $0.3x10^6$, $1.5x10^6$, and $2.0x10^6$ cells/mL, Tables A-C in S1 File). As the initial cell seeding density was increased from $0.3x10^6$ cell/mL to 0.6, 1.0, 1.5 and $2x10^6$ cells/mL, cell number after 9 days increased from 0.12±0.04 cells/mL to 2.1±0.2, 4.8±0.3, 4.5±0.4, and 5.8±0.4 cells/mL, respectively, whereas the CD44 marker expression changed from 0.6±0.1 to 25.0±1.6, 29.0±1.7, 3.3±0.9, and 3.2±0.8. Further, the expression of CD44, ABCG2, and EGFR markers after 9 days was significantly higher than day 6 (Fig 1C–1E).

E-cadherin mRNA expression of the encapsulated cells (Fig 1F) did not increase with incubation time for initial cell densities of $0.3x10^6$, $0.6x10^6$, and $1x10^6$ cells/mL but the expression increased significantly at higher cell densities of $1.5x10^6$ and $2x10^6$ cells/mL (Fig 1F, significantly higher than those groups with initial cell density of $0.3x10^6$, $0.6x10^6$, and $1.0x10^6$ cells/mL, Table D in S1 File). E-cadherin mRNA expression for the initial cell seeding density of $1.5x10^6$ cells/mL increased from 1.9±0.7 to 6.6±1.7 and 24.2±2.7 after 2, 4 and 6 days of incubation, respectively, whereas the expression increased from 3.7±0.9 to 21.4±1.8 and 40.3±3.2 at the higher seeding density of $2x10^6$ cells/mL. The encapsulated MDA231 cells with initial cell seeding density of $0.6x10^6$ cells/mL formed slightly lower number of spheres compared to the density of $1.0x10^6$ cells/mL. Therefore to minimize cell aggregation, all subsequent experiments were done with the initial cell seeding density of $0.6x10^6$ cells/mL.

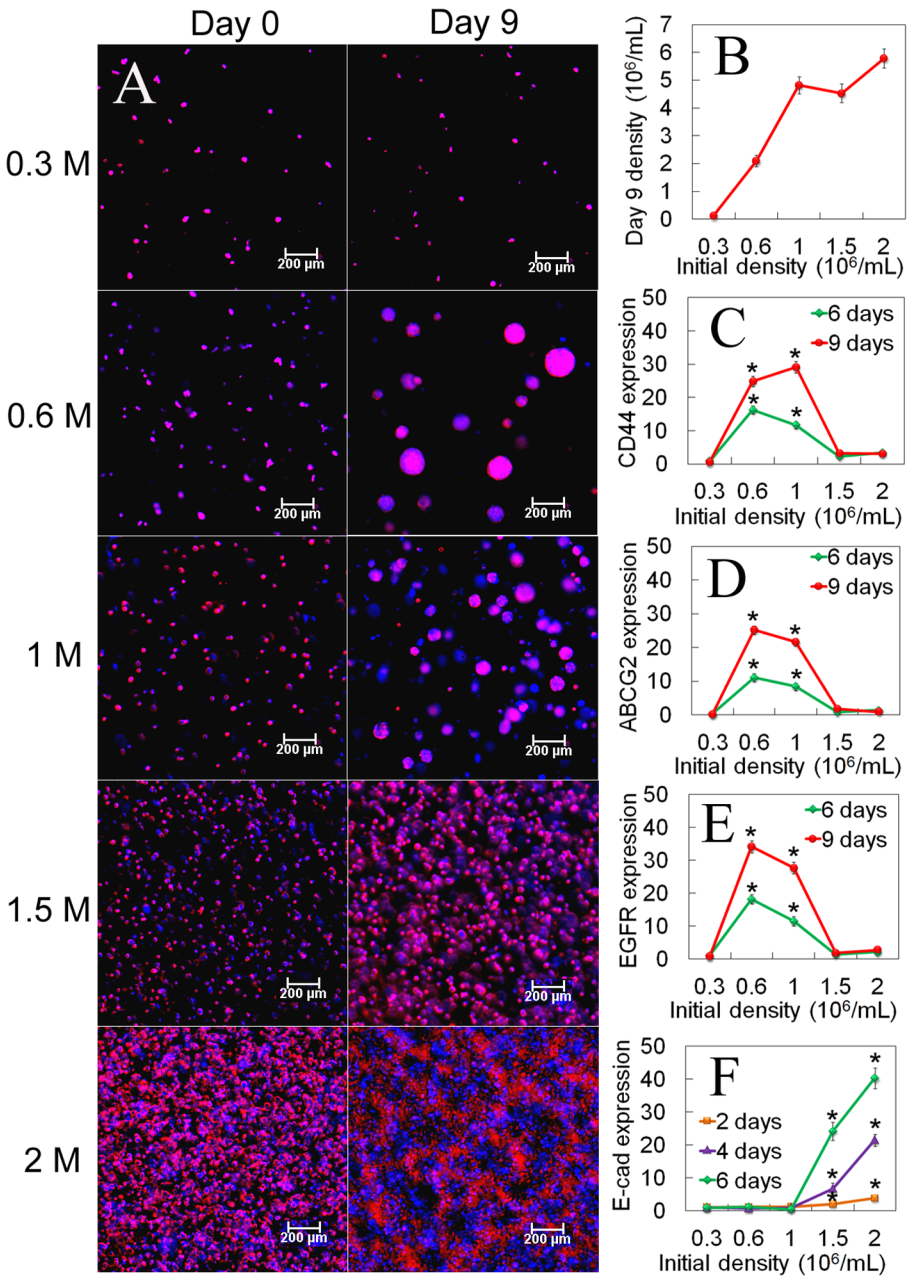

Fig 1. Dependence of tumorsphere growth on initial seeding density of MDA231 cells. (A) DAPI (blue) and phalloidin (red) stained images of the encapsulated MDA231 cells (5 kPa gel) on day zero (left column) and after 9 days of incubation (right column) versus initial number of cells; (B) Number of encapsulated cells after 9 days of incubation as a function of initial cell number; mRNA expression of CD44 (C), ABCG2 (D), and EGFR (E) markers of the encapsulated cells after 6 and 9 days of incubation as a function of initial cell number; (F) E-cadherin mRNA expression of the encapsulated cells after 2, 4 and 6 days of incubation as a function of the initial cell number. The scale bars in (A) are 200 μm. An asterisk in (C-E) indicates a statistically higher ($p<0.05$) mRNA expression in the test group compared to those groups with initial cell density of $0.3x10^6$, $1.5x10^6$, and $2.0x10^6$ cells/mL at the same time point. An asterisk in (F) indicates a statistically higher E-cad expression in the test group compared to those groups with initial cell density of $0.3x10^6$, $0.6x10^6$, and $1.0x10^6$ cells/mL at the same time point. The p-values for the asterisks in (C-F) are listed in Tables A-D in S1 File. Error bars correspond to means±1 SD for n = 3.

doi:10.1371/journal.pone.0132377.g001

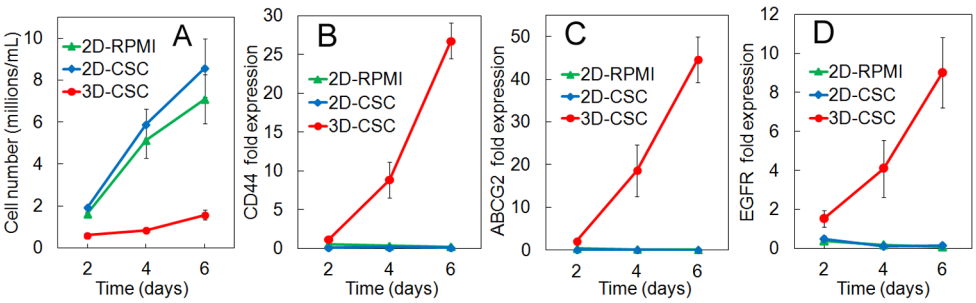

Fig 2. Dependence of tumorsphere growth on culture medium in 2D versus 3D for MDA231 cells. Number density (A) and mRNA expression of CD44 (B), ABCG2 (C), and EGFR (D) markers for MDA231 cells as a function of incubation time. Groups included cells on 2D adherent plates and cultured in RPMI-1640 medium (2D-RPMI), cells on 2D plates and cultured in CSC medium (2D-CSC), and cells encapsulated in the 5 kPa PEGDA gel and cultured in CSC medium (3D-CSC). An Asterisk in (A) indicates a statistically lower ($p<0.05$) cell number in the test group compared to 2D groups at the same time point. An Asterisk in (B-D) indicates a statistically higher ($p<0.05$) mRNA expression in the test group compared to 2D groups at the same time point. The p-values for the asterisks in (A-D) are listed in Tables E-H in S1 File. Error bars correspond to means±1 SD for n = 3.

doi:10.1371/journal.pone.0132377.g002

Dependence of tumorsphere growth on culture medium in 2D and 3D

Groups included MDA231 cells on 2D adherent plates and cultured in RPMI-1640 medium (2D-RPMI), cells on 2D plates and cultured in CSC medium (2D-CSC), and cells encapsulated in the 5 kPa PEGDA gel and cultured in CSC medium (3D-CSC). Cell numbers increased for all groups with incubation time but the increase was higher for the 2D groups (Figs 2A and 3D-CSC group statistically lower cell number than the 2D groups, Table E in S1 File). For any time point, the cell number for 2D-CSC group was slightly higher than 2D-RPMI but the difference was not statistically significant. For any time point, the cell number for 3D-CSC was significantly lower than the 2D groups because cell growth in the non-adherent PEGDA gel was limited to the stem cell sub-population. The expression of CD44, ABCG2, and EGFR CSC markers in the 2D groups (blue and green curves) did not increase with incubation time and the difference in marker expression between 2D-1640 and 2D-CSC groups was not significant (Fig 2B–D). The expression of CSC markers for the cells in 3D-CSC group was much higher than those in 2D groups (red curve Fig 2B–D, statistically higher than the 2D groups, Tables F-H in S1 File). The results in Fig 2 demonstrated that the higher expression of CSC markers for cells in 3D-CSC group was related to the encapsulation of cancer cells in PEGDA gel, not the change in culture medium.

Dependence of tumorsphere growth on niche size

Micropatterning was used to control average tumorsphere size in the gel (Fig 3A). Fluorescent images of cellTracker-stained MDA231 cells in the 5 kPa circular gel patterns with diameters of 50 to 250 μm showed uniform cell seeding 2 days after encapsulation (Fig 3B–3F). DAPI and phalloidin-stained images of the tumorspheres grown in the patterns with diameters of 50 to 250 μm are shown in Fig 3G–3K. It should be noted that the seven tumorspheres shown in each image (G-K) are from multiple patterns in the gel sample, not a single pattern, to show size range and shape of the tumorspheres for a given pattern size. Cell number (Fig 3L) and average tumorsphere size (Fig 3M) increased steadily with incubation time and pattern size. For the measurement of cell density in the patterned gels (Fig 3L), the sample size was normalized to the initial cell seeding density in the gels. We speculate that after cell seeding the CSC sub-population grew whereas the differentiated cells that relied on cell-matrix interaction did

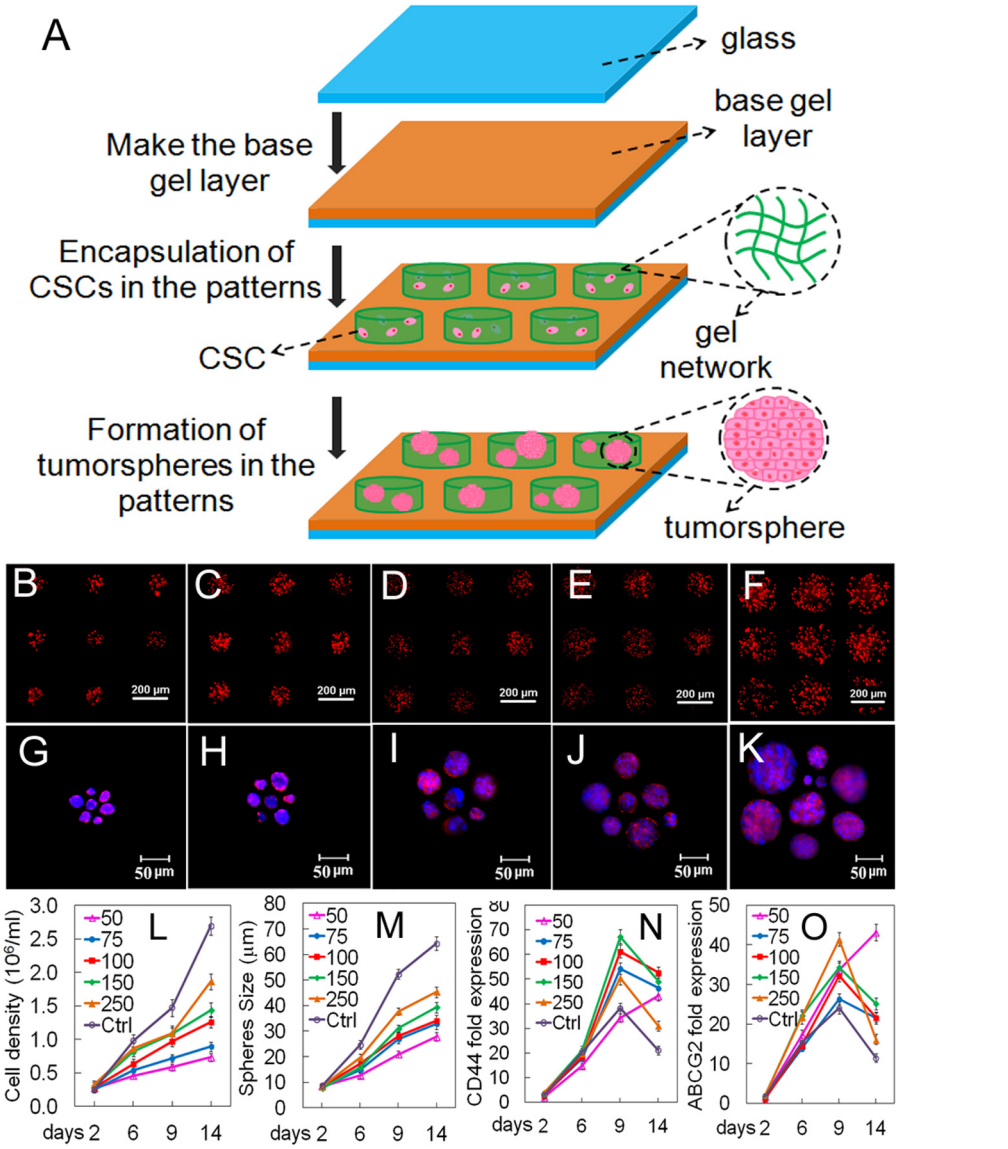

Fig 3. Dependence of tumorsphere growth on niche size for MDA231 cells. (A) Procedure for cell encapsulation in the micropatterned gel. CellTracker stained images of MDA231 cells encapsulated in the 5 kPa gel with circular patterns with diameter of 50 (B), 75 (C), 100 (D), 150 (E), and 250 (F) μm after 2 days of incubation (scale bars in B-F are 200 μm). DAPI (blue) and phalloidin (red) stained images of 7 representative tumorspheres formed by the encapsulated cells in (B-F) from different sections of the patterned gels after 14 days of incubation with 50 (G), 75 (H), 100 (I), 150 (J), and 250 (K) μm patterns (scale bars in G-K are 50 μm). Note that the 7 representative tumorspheres in (G-K) are from multiple patterns in the gel sample, not a single pattern, to show size range and shape of tumorspheres for a given pattern size. Cell number (L), average tumorsphere size (M), CD44 expression (N), and ABCG2 expression (O) of the cells in (B-F) with incubation time for 50 (pink), 75 (blue), 100 (red), 150 (green), 250 (brown) μm patterns, and un-patterned gel (purple). Error bars in (L-O) correspond to mean±1 SD for n = 3.

doi:10.1371/journal.pone.0132377.g003

not grow in the non-adherent PEGDA gel. As a result, the cell density decreased slightly after two days of incubation (Fig 3L). As the encapsulated CSCs grew and formed tumorspheres in the gel, the measured cell density increased to values greater than the initial seeding density of $0.6x10^6$ cells/mL. CD44 (Fig 3N) and ABCG2 (Fig 3O) marker expressions of tumorspheres formed in the un-patterned gel and those gels with 75–250 μm patterns initially increased with

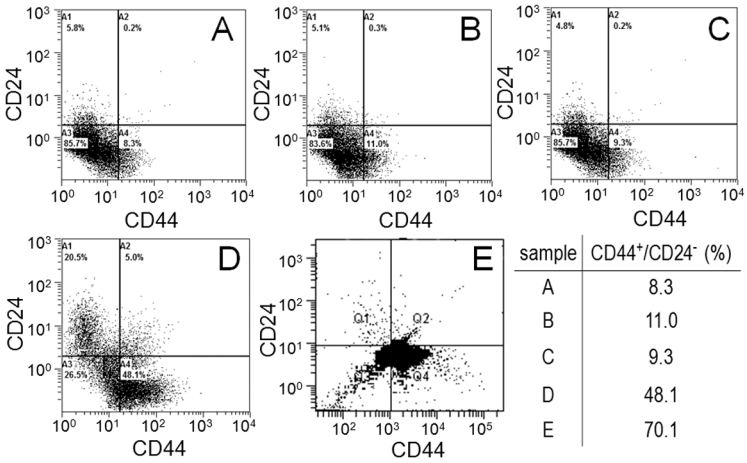

Fig 4. CSC fraction of MDA231 cells encapsulated in the patterned 5 kPa gel. MDA231 cells cultured on adherent tissue culture plate (TCP, A), non-adherent tissue culture plate (suspension, B), by encapsulation in Matrigel (C), encapsulation in un-patterned 5 kPa PEGDA gel (D), and encapsulation in 50 μm patterned 5 kPa PEGDA gel; (F) CSC fraction of the MDA231 cells in (A-E) as the sub-population of cells in the fourth quadrant ($CD44^+/CD24^-$).

doi:10.1371/journal.pone.0132377.g004

incubation time, peaked on day 9, and then decreased. On the other hand, marker expression of those tumorspheres formed in the 50 μm patterned gel steadily increased with incubation time for 14 days (pink line in Fig 3N and 3O). CD44 marker expression of tumorspheres in the 150 μm patterned gel changed from 3.7±0.5 to 21±2, 67±3, and 49±2 after 2, 6, 9, and 14 days, respectively, whereas CD44 expression of those tumorspheres in the 50 μm patterned gel changed from 2.1±0.7 to 15±1, 34±2, and 43±2. Based on micropatterning results, expression of CSC markers for MDA231 cells depended on tumorsphere size and 50 μm size spheres had highest expression of CSC markers. Therefore, in all subsequent experiments cancer cells were encapsulated in un-patterned gels but the incubation time was limited to 9 days to control the average tumorsphere size.

Flow cytometry was used to quantify the CSC fraction ($CD44^+/CD24^-$) of MDA231 tumorspheres grown in 5 kPa PEGDA gel [35]. The gel modulus for MDA213 cells is optimized with respect to tumorsphere formation in the following section on "Dependence of optimum matrix stiffness for CSCs on tissue origin." As only MDA231 cells were used, all PEGDA-encapsulated tumorspheres (un-patterned and patterned) for flow cytometry experiments were grown in the 5 kPa gel. Groups included cells cultured on adherent tissue culture plate (TCP, Fig 4A), cells on non-adherent TCP (suspension culture, Fig 4B), cells encapsulated in Matrigel with 500 Pa stiffness [36] (Fig 4C), cells encapsulated in the un-patterned 5 kPa PEGDA gel (Fig 4D), and in the 50 μm patterned gel (Fig 4E). All groups were cultivated for 8 days. CSC fraction of MDA231 cells cultured on adherent plates was 8.3% close to the previously reported CSC fraction [37], which increased slightly to 11% by suspension culture and 9.3% by encapsulation in Matrigel. Encapsulation of MDA231 cells in the 5 kPa un-patterned and 50 μm patterned gels markedly increased the CSC fraction to 48% and 70%, respectively.

Dependence of optimum matrix stiffness for CSCs on tissue origin

The effect of tissue origin on optimum matrix stiffness for growth and expression of CSC markers was investigated with MCF7 and MDA231 breast, HCT116 colorectal, AGS gastric, and U2OS osteosarcoma cells encapsulated in PEGDA gels with compressive modulus ranging from 2 to 70 kPa. Non-tumorigenic MCF10A cells did not form tumorsphere (first column in

Fig 5A) whereas all cancer cells formed tumorspheres after 9 days of encapsulation in the gel (Fig 5A). The increase in cell number, sphere number and sphere size with incubation time depended on cancer cell type (Fig 5B–5D). 20% of the MCF7 tumorspheres had 60–80 μm size range compared to 75% for MDA231 in the 5 kPa gel (Fig 5E). 10% of the poorly-invasive AGS tumorspheres had 40–60 μm size range compared to 70% for the moderately-invasive HCT116 in the 25 kPa gel (Fig 5E). 70% of the moderately-invasive U2OS tumorspheres in the 50 kPa gel had sizes <40 μm (Fig 5E). The cell number of triple-negative (claudin-low) MDA231 and luminal-A MCF7 breast cancer cells [38] after 9 days encapsulation in the 5 kPa gel was 1.6± 0.1x10^6 and 1.0±0.1x10^6 cells/mL, respectively; the tumorsphere size was 56±4 and 33±3 μm, and the sphere number density was 5.4±0.3x10^3 and 2.3±0.3x10^3 spheres/mm^3 (Fig 5B–5D). MDA231 and MCF7 cells have a similar doubling time of 38 h, as reported by the supplier (ATCC, Manassas, VA). The average invasion rate of MDA231 and MCF7 cells in collagen type I matrix, measured by Sakai et al. [39], was 31 and 20 μm, respectively, after 18 h of incubation. Hence, the data indicates a possible relation between the growth rate of tumorspheres in the gel at the optimum modulus for breast cancer cells and the cell invasion rate in collagen I matrix.

The dependence of cell number, sphere number, and average sphere size on modulus for all cancer cells was bimodal (Fig 5B–5D). The optimum gel modulus with respect to tumorsphere growth and expression of CSC markers was 5 kPa for MCF7 and MDA231 breast cancer cells, 25 kPa for HCT116 and AGS gastrointestinal cells, and 50 kPa for U2OS osteosarcoma cells (Fig 5B–5D, statistically higher than the other moduli for a given cell type, Tables I-K in S1 File). For example, number of MDA231 tumorspheres after 9 days incubation in the gels with 2, 5, 25, 50, and 70 kPa modulus was 1.6±0.2, 5.4±0.3, 1.2±0.2, 0, and 0 spheres/mm^3 whereas for U2OS cells it was 0, 0, 0.05±0.01, 0.77±0.25, and 0 spheres/mm^3. Expression of CD44 marker was used to characterize the CSC sub-population of all cancer cells [40]. ABCG2 expression was used as the second marker for MCF7 CSCs [32], EGFR for MDA231 CSCs [34], TGF-β for HCT116 CSCs [41], OCT4 for AGS CSCs [42], and CD133 for U2OS CSCs [43]. Expression of CSC markers for cancer cells encapsulated in PEGDA gel as a function of modulus (Fig 5F) was consistent with cell densities, tumorsphere sizes and number densities in Fig 5B–5D. For time points of 6 and 9 days, optimum gel modulus with respect to the expression of CSC markers was 5 kPa for MCF7 and MDA231 cells, 25 kPa for HCT116 and AGS cells, and 50 kPa for U2OS cells (Fig 5F, statistically higher than the other moduli for a given cell type and at a given time, Tables L-U in S1 File). CD44 glycoprotein is involved in cell-cell adhesion of CSCs [44] and the CD44 binding peptide RLVSYNGIIFFLK (CD44BP) [45] conjugated to the 5 kPa PEGDA gel abolished tumorsphere formation in 4T1 and MCF7 breast cancer cells [17]. Fig 6 shows the effect of CD44BP conjugation to PEGDA gel on tumorsphere formation by the encapsulated cancer cells from different tissues at the optimum gel modulus (5 kPa for MDA231, 25 kPa for HCT116, and 50 kPa for U2OS). Groups included the gel without CD44BP (Ctrl), with conjugated mutant-CD44BP (mCD44BP), and with conjugated CD44BP. MDA231, HCT116, and U2OS cells encapsulated in the gel without peptide formed tumorspheres (images A, C and E in Fig 6) whereas those encapsulated in the CD44BP-conjugated gel did not (images B, D and F in Fig 6). Cell number (Fig 6G), average tumorsphere size (Fig 6H), and sphere number (Fig 6I) of all cell types increased in the gel without peptide (blue bars in G-I) or the gel with mutant peptide conjugation (orange bars in G-I) after 9 days incubation. Conversely MDA231, HCT116 or U2OS cells did not grow and did not form tumorspheres in the CD44BP-conjugated gel (green bars in Fig 6G–6I, statistically lower than those groups without CD44BP conjugation or with mutant CD44BP conjugation, Tables A-C in S2 File). In the CD44BP-conjugated gel, MDA231 cells did not express CSC markers CD44 and EGFR after 9 days incubation, HCT116 cells did not express CD44 and TGF-β markers, and U2OS

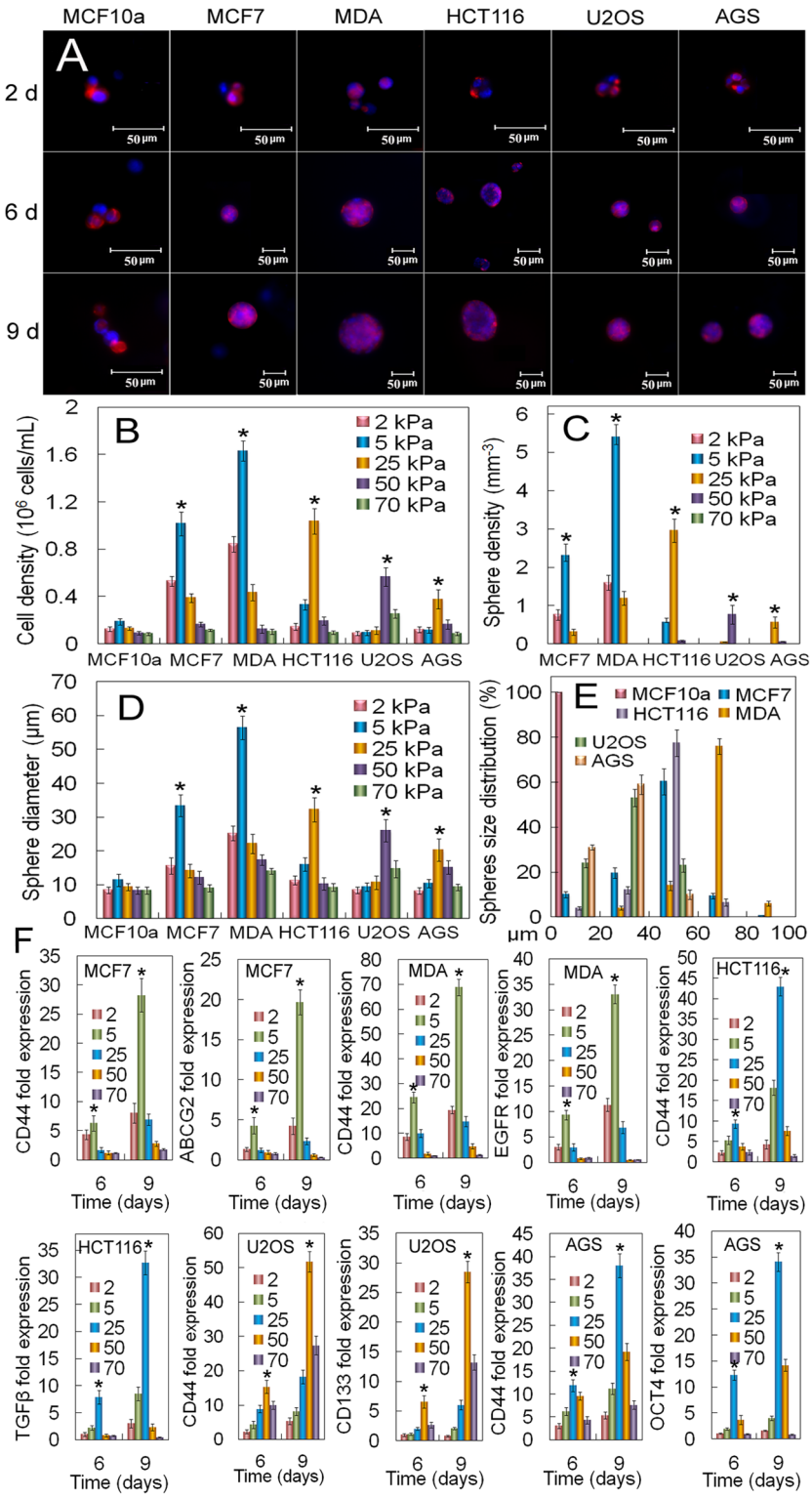

Fig 5. Dependence of the optimum gel modulus for CSC growth on tissue origin of cancer cells. (A) DAPI (blue) and phalloidin (red) stained images of MCF10A, MCF7, MDA231, HCT116, U2OS, and AGS cancer cells encapsulated in the un-patterned gels after 2, 6, and 9 days of incubation (scale bars in A are 50 μm). Cell number (B), tumorsphere number (C), tumorsphere diameter (D), and tumorsphere size distribution (E) as a function of cancer cell type after 9 days of encapsulation for gel moduli of 2 (pink), 5 (blue), 25 (brown), 50 (purple), and 70 (green) kPa. The gel modulus in (A and E) was the optimum PEGDA

modulus of 5 kPa for MCF7 and MDA231 cells; 25 kPa for HCT116 and AGS; 50 kPa for U2OS. (F) mRNA expression of CSC markers for MCF7 (CD44 and ABCG2), MDA231 (CD44 and EGFR), HCT116 (CD44 and TGF-β), U2OS (CD44 and CD133), and AGS (CD44 and OCT4) after 6 and 9 days of encapsulation for gel moduli of 2 (pink), 5 (blue), 25 (brown), 50 (purple), and 70 (green) kPa. An asterisk in (B-D) indicates a statistically higher ($p<0.05$) cell number, sphere number and size for the test modulus compared to all other moduli for a given cell type. An asterisk in (F) indicates a statistically higher ($p<0.05$) marker expression level for the test modulus compared to all other moduli for a given cell type and at a given time. The p-values for the asterisks in (B-D,F) are listed in Tables I-U in S1 File. Error bars correspond to mean±1 SD for n = 3.

doi:10.1371/journal.pone.0132377.g005

cells did not express CD44 and CD133 markers (Fig 6J–6L, statistically lower than those groups without CD44BP conjugation or with mutant CD44BP conjugation, Tables D-F in S2 File). According to the results in Fig 6, ligand inhibition of CD44 abolished growth and expression of CSC markers in vitro in cancer cells from breast, colorectal, and bone tissues encapsulated in PEGDA gel with optimum stiffness.

Epithelial to mesenchymal transition and Hippo transducers

mRNA expression of EMT markers for MDA231 cells encapsulated in the un-patterned 5 kPa gel is shown in Fig 7A–7H). As incubation time was increased from day 2 to 6, E-cadherin expression of the cells decreased initially reaching a minimum on day 3 whereas the expression of N-Cadherin, Snail, Twist, Vim, and ZEB2 was bimodal with a peak value on day 4 with the exception of slug which peaked on day 3 (Fig 7A and 7B, 7D–7H, statistically lower in A and higher in B,D-H than all other time points, Tables G-M in S2 File). Expression of TGF-β steadily increased with incubation time (Fig 7C). The expression of pYAP, total YAP, and YAP/TAZ transcription factors for MDA231 cells encapsulated in the un-patterned gel as a function of gel modulus is shown in Fig 7I–7K) after 6 days of incubation. Expression of pYAP was lowest and that of YAP/TAZ was highest for tumorspheres in the 5kPa gel as compared to those in 2.5 and 25 kPa (Fig 7I and 7K, statistically lower in I and higher in K than the other two moduli, Tables N,O in S2 File).

Discussion

Unlike natural biomolecules like collagen that are amphiphilic and partially phase separate in aqueous solution to form a microporous structure, PEGDA gels form a homogenous molecular mesh. The water content of PEGDA gels used in this work was >80% and the calculated mesh sizes (93–34 nm for the gels with 2.5–50 kPa modulus [46]) were at least an order of magnitude larger than the size of proteins [47]. Thus diffusion of the components of the culture medium was not blocked by the PEGDA mesh. Based on previous reports [48], large proteins (as large as 10 nm in diameter) can diffuse without limitation through the PEGDA mesh. We previously showed that cancer cells steadily grow in cell number with incubation time (for up to 14 days) in PEGDA gels and form tumorspheres as large as 250 μm in diameter without diffusion limitation [16]. In this work, the initial cell density with respect to tumorsphere formation was minimized (Fig 1) in order to reduce the consumption rate of nutrients and oxygen in the gel. The minimum initial cell density allowed each encapsulated cancer stem cell to form a colony in the gel without interference from other cells in the matrix. The results of this work show that under equal conditions (cell density, gel structure and mesh size, gel composition, culture medium composition), the optimum modulus for the growth and expression of CSC markers by tumorspheres grown in the PEGDA gel was dependent on tissue origin of the cancer cells.

It is reported that disruption of TGF-β signaling inhibited activation of epithelial to mesenchymal transition (EMT) in primary mammary epithelial cells and reduced metastasis [49]. Recent reports indicate that NF-kB signaling in basal-type triple-negative breast cancer cells

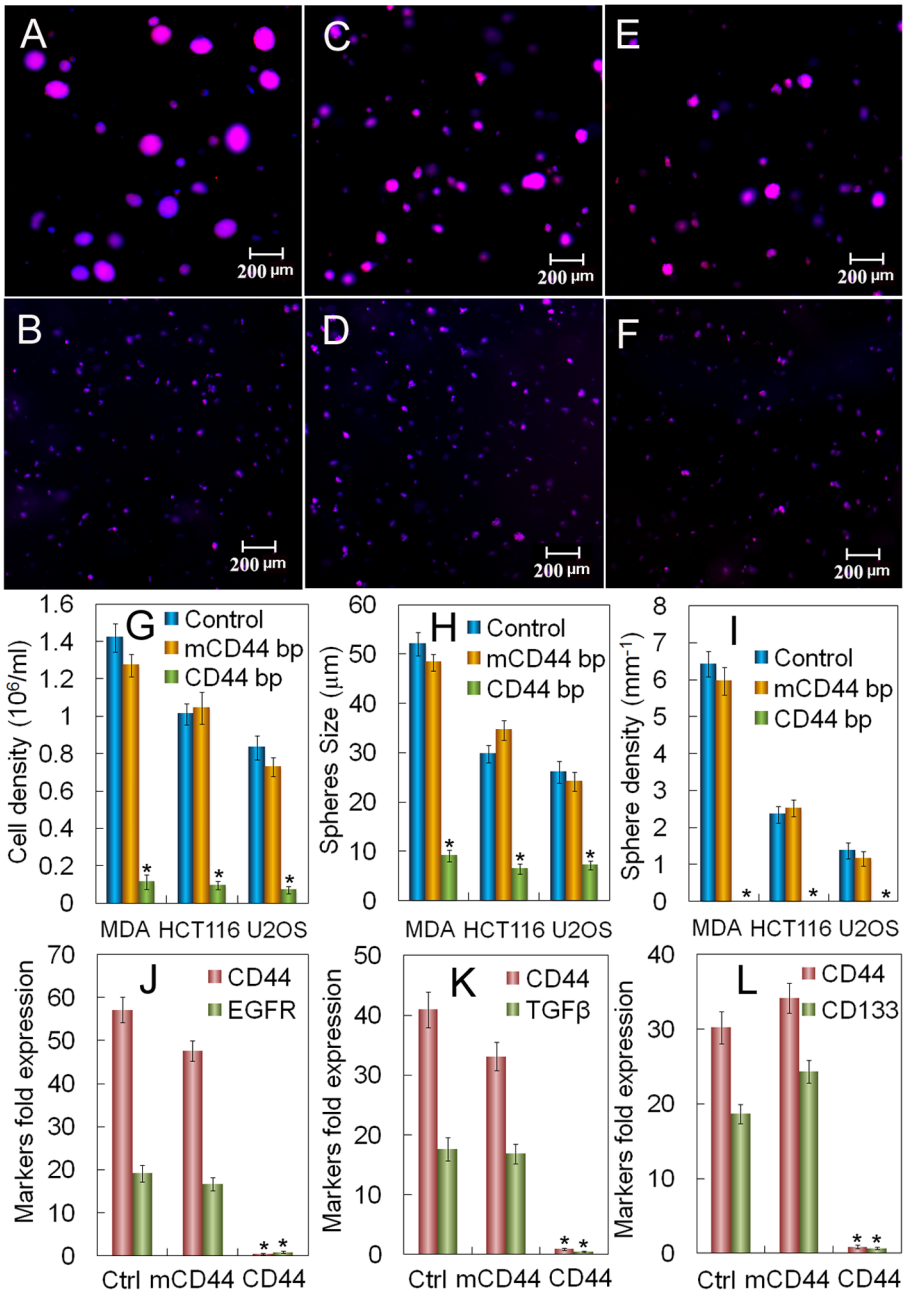

Fig 6. Dependence of tumorsphere growth on conjugation of CD44 binding peptide to the gel. (A) DAPI (blue) and phalloidin (red) stained images of MDA231 (A+B), HCT116 (C+D), and U2OS (E+F) cells encapsulated in the un-patterned gel with optimum modulus (5 kPa for MDA231, 25 kPa for HCT116, and 50 kPa for U2OS) without CD44BP (A+C+E) and with CD44BP conjugation (B+D+F) after 9 days incubation (scale bar in A-F is 200 μm). The initial seeding density of all cell types in the gel was $0.6x10^6$ cells/mL. Cell number (G), tumorsphere size (H), and tumorsphere number (I) for MDA231, HCT116, and U2OS cells encapsulated in the gel without (blue) and with (green) conjugated CD44BP and with conjuagted mutant-CD44BP (mCD44BP, orange) after 9 days incubation. mRNA expression of CSC markers for MDA231 (J, CD44 and EGFR), HCT116 (K, CD44 and TGF-β), and U2OS (L, CD44 and CD133) encapsulated in the gel without conjugation, with mCD44BP, and with CD44BP conjugation. An Asterisk in (G-L) indicates a statistically lower cell number, sphere number and size, and marker expression for the test group compared to those groups without CD44BP conjugation and with mutant CD44BP conjugation of the gel for a given cell type. The p-values for the asterisks in (G-L) are listed in Tables A-F in S2 File. Error bars correspond to mean±1 SD for n = 3.

doi:10.1371/journal.pone.0132377.g006

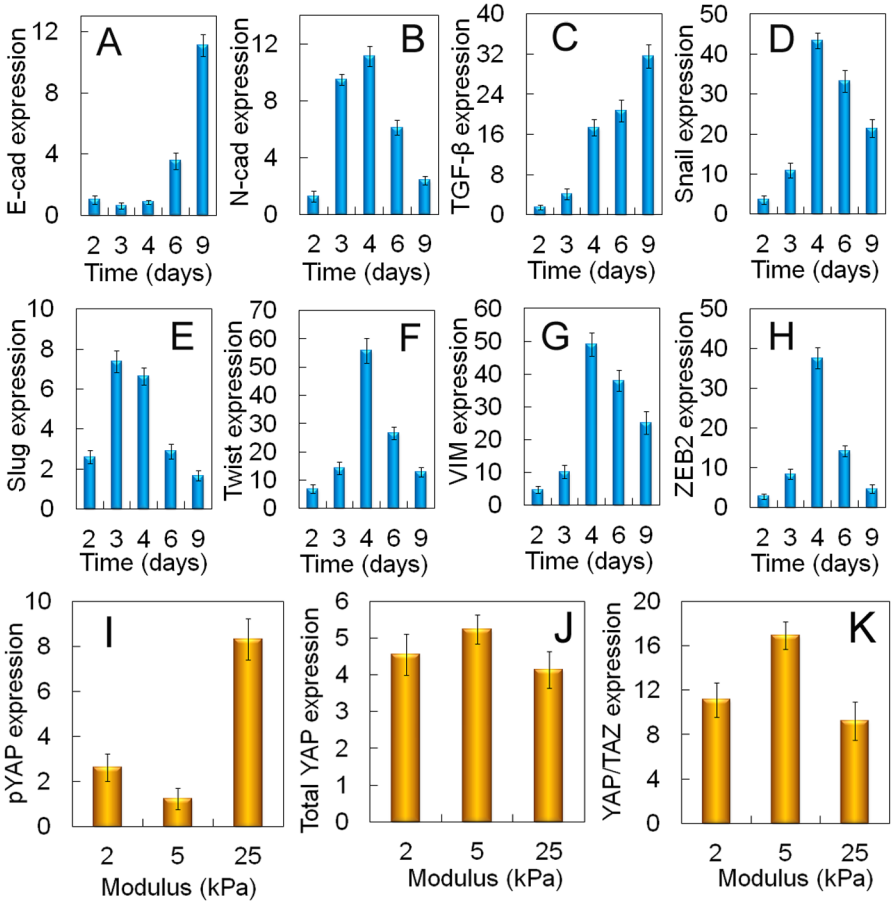

Fig 7. Dependence of tumorsphere growth on EMT marker expression for MDA231 cells. mRNA expression of EMT markers E-cadherin (A), N-cadherin (B), TGF-β (C), Snail (D), Slug (E), Twist (F), Vimentin (G), and ZEB2 (H) for MDA231 cells encapsulated in the un-patterned 5 kPa gel as a function of incubation time. Protein expression of pYAP (I), total YAP (J), YAP/TAZ (K) for the MDA231 cells encapsualted in the un-patterned gel as a function of modulus after 6 days of incubation. An asterisk in (A) indicates a statistically lower marker expression for that time point compared to all other time points. An asterisk in (B,D-H) indicates a statistically higher marker expression for that time point compared to all other time points. An asterisk in (I) indicates a statistically lower protein expression for that modulus compared to the other two moduli. An asterisk in (k) indicates a statistically higher protein expression for that modulus compared to the other two moduli. The p-values for the asterisks in (A,B,D-I,K) are listed in Tables G-O in S2 File. Error bars correspond to mean±1 SD for n = 3.

doi:10.1371/journal.pone.0132377.g007

up-regulated the expression of soluble Jagged-1 in non-CSCs in the tumor microenvironment, which in turn stimulated Notch activity in CSCs by paracrine signaling and led to CSC growth [50]. Jagged-1 released by endothelial cells in the tumor microenvironment had a paracrine effect on the growth of colorectal CSCs via Notch activation [51]. Breast CSCs also expanded and proliferated by estrogen or fibroblast growth factor-9 (FGF-9) signaling through the paracrine FGF/FGFR/TbX3 pathway [52]. Therefore, the absence of tumorsphere formation by MDA231 cells encapsulated in the gel with initial density of $0.3x10^6$ cells/mL (Fig 1) can be attributed to reduced paracrine signaling at low cell densities.

Bimodal expression of CSC markers with incubation time for tumorspheres formed in the 75–250 μm patterned gels may be related to a shift in polarity of cell division. For the 50 μm patterned gel, CSC marker expressions increased steadily with incubation time because the relatively small patterns kept the tumorsphere size below the threshold required to shift the

polarity of cell division. This is consistent with the growing evidence that geometrical confinement affects self-renewal, differentiation, and gene expression of normal and malignant cells [42]. In that respect, confinement of human cervical carcinoma cells changed the average tumorsphere size and increased asymmetric cell division [53], cluster size affected proliferation of MCF10A cells [43], and patterning enhanced differentiation of neural stem cells [44]. The measurement of the polarity of cell division is complicated by the fact that stemness in cancer cells can be gained or lost in tumor cells [54], thus its quantification requires CSCs that fluoresce under the control of a CSC marker gene. The dependence of polarity of cell division on tumorsphere size is beyond the scope of this manuscript and will be investigated in the future.

According to the data in Fig 5, the optimum stiffness was dependent on the cancer cells' tissue origin. That optimum modulus was 5 kPa for all breast cancer cells (4T1, MCF7, and MDA231), 25 kPa for gastrointestinal cancer cells (HCT116 and AGS), and 50 kPa for U2OS osteosarcoma cells. The reported modulus of the breast tumor tissue depends on malignancy and mode of measurement, but all reports indicate that breast tumors have a significantly higher stiffness than the normal tissue [55]. Paszek et al. measured the unconfined compressive modulus of normal and cancerous breast tissue of MMTV-Her2/neu, Myc, and Ras transgenic mice and reported an average modulus of 170±30 Pa for the normal tissue, 920±270 Pa for the stroma attached to the tumor tissue, and 4050±940 Pa for the tumor tissue [11]. In another study, the growth rate of MDA231 cells in 2D reached a maximum as the substrate stiffness increased from 150 to 4800 Pa and did not change with further increase to 9600 Pa [56]. Considering the wide range of stiffness values reported for breast tumor tissue, our optimum gel modulus of 5 kPa for breast cancer cells with respect to growth and expression of CSC markers (Fig 5) is very close to the reported value by Paszek et al. [11]. Tang et al. reported that human HCT8 colorectal carcinoma cells cultivated on soft (1 kPa), stiff (21–47 kPa), and very stiff (3.6 GPa) 2D substrates exhibited a metastatic phenotype only on the substrate with the intermediate stiffness [18], close to the optimum gel modulus of 25 kPa in our experiments for HCT116 cells. Mylona et al. measured highest cell area for osteosarcoma cells isolated from human femur on the 55 kPa collagen type I coated polyacrylamide gels [19], close to the optimum modulus of 50 kPa in our experiments with U2OS osteosarcoma cells.

The number of tumorspheres increased considerably at the optimum gel modulus for all cancer cells (Fig 5C). For example for MDA231 cells, the sphere number increased from 1600± 200/mL at 2 kPa gel to 5400±330/mL at 5 kPa and then decreased to 1200±180/mL and zero as the gel modulus was increased to 25 and 50 kPa, respectively. Based on the FACS data (Fig 4), CSC fraction of MDA231 cells increased from 11% in suspension culture to 48% in the 5 kPa gel. One pathway to transform cancer cells into CSCs is epithelial to mesenchymal transition (EMT) [5,57]. The hallmark of EMT is the decreased expression of E-cadherin and increased expression of N-Cadherin [58]. Other EMT markers include Snail, Slug, Twist, ZEB2, TGF-β, and vimentin (Vim) [59,60]. E-cadherin expression of MDA231 cells encapsulated in the unpatterned 5 kPa gel had a minimum on day 3 (Fig 7A) whereas the expression of N-cadherin, Snail, Slug, Twist, Vim, and ZEB2 was bimodal with a peak on day 4 with the exception of slug which peaked on day 3 (Fig 7B and 7D–7H). TGF-β an inducer of primary tumorigenesis and a positive regulator of tumor progression [61] increased with incubation time (Fig 7C). One pathway for the involvement of TGF-β in EMT is the activation of Smads via ALK-5 receptor which in turn induces the autocrine production of TGF-β leading to EMT amplification [61]. Activation of Smads can mediate the action of β-catenin and LEF, leading to the activation of TGF-β/Smad/LEF/PDGF pathway to reinforce EMT. Another pathway is the TGF-β-induced activation of p38 MAPK and RhoA mediated by β1 and αVβ6 integrin receptors which leads to autocrine TGF-β production and EMT induction [61].

Activation of EMT is in response to the innate ability of cancer cells to grow and invade. We speculate that a sub-population of the encapsulated cancer cells in the gel formed a confluent cell layer held together by cell-cell interaction. Since the PEGDA gel was non-degradable, we further speculate that a fraction of the confluent cells underwent EMT, as shown by the up-regulation of EMT markers (Fig 7) and grew to form tumorspheres by pushing against the retractive force of the gel matrix. In other words, the cells in the tumorsphere had to push against the elasticity of the gel network to create free volume for cell growth. A gel with higher compressive modulus required a greater force by the encapsulated cells to create free volume for cell growth. Therefore, mechanotransduction may have played a role in the growth of tumorspheres in the gel with incubation time.

Previous studies show a link between the Hippo transducers and CSC growth via the Yes-associated protein and its transcriptional co-activator with PDZ-binding motif (YAP/TAZ) in cancer cells during EMT [62]. Dephosphorylation and localization of YAP/TAZ to the nucleus in mammary epithelial cells seeded on polyacrylamide hydrogels depended on substrate stiffness [63]. Upstream regulators of the Hippo transducers include the G protein-coupled receptors (GPCRs, G12/13), regulated by lipid rafts on the cell surface, that change conformation in response to the elastic force exerted by the matrix [64,65]. The conformational change leads to dephosphorylation of YAP/TAZ, their nuclear localization, and CSC growth [63,64]. The expression of pYAP was lowest (Fig 7I) and YAP/TAZ protein expression was highest (Fig 7K) for MDA231 tumorspheres grown in the 5kPa gel as compared to those at 2.5 and 25 kPa. We speculate that the higher expression of YAP/TAZ transcription factors at the optimum modulus of PEGDA gels led to the expression of genes responsible for EMT and up-regulation of CSC markers in MDA231 cancer cells.

In summary, regulation of CSC niche depends on many factors in the tumor microenvironment including tissue type, matrix stiffness, niche size and its ECM composition, supporting stroma cells as well as the local pH, oxygen partial pressure, and other culture conditions [66]. Our results demonstrate that the optimum matrix stiffness for growth and expression of CSC markers is dependent on tissue origin of tumor which was 5 kPa for breast, 25 kPa for colon and stomach, and 50 kPa for bone. Further, the optimum tumorsphere size with respect to the expression of CSC markers was 50 μm.

Conclusions

In this work, the effect of cells' tissue origin on growth and marker expression of the CSC sub-population of cancer cells was investigated with human breast MCF7 and MDA231, colorectal HCT116, gastric AGS, and bone U2OS cancer cells. Micropatterning experiments revealed that growth and expression of CSC markers of tumor cells encapsulated in PEGDA gel was dependent on average tumorsphere size with 50 μm optimum size. The optimum matrix modulus for growth and expression of CSC markers was 5 kPa for MCF7 and MDA231 cells, 25 kPa for HCT116 and AGS, and 50 kPa for U2OS cells. Further, the expression of EMT markers for cancer cells encapsulated in the gel with optimum modulus increased in the first 3–4 days of incubation indicating that a sub-population of cancer cells underwent EMT to acquire the CSC phenotype. The expression level of YAP/TAZ transcription factors for the encapsulated cancer cells was highest at the optimum stiffness indicating a link between the Hippo transducers and CSC growth. The marker expression results suggest that the CSC sub-population of cancer cells resides within a niche with optimum stiffness which depends on the cancer cells' tissue origin.

Supporting Information

S1 File. Tables of p-values for statistically significant differences for the data with an asterisk in Figs 1, 2 and 5. P-values for Fig 1C days 6 and 9 (Table A); P-values for Fig 1D days 6 and 9 (Table B); P-values for Fig 1E days 6 and 9 (Table C); P-values for Fig 1F days 2, 4, and 6 (Table D); P-values for Fig 2A (Table E); P-values for Fig 2B (Table F); P-values for Fig 2C (Table G); P-values for Fig 2D (Table H); P-values for Fig 5B (Table I); P-values for Fig 5C (Table J); P-values for Fig 5D (Table K); P-values for Fig 5F for MCF7-CD44 (Table L); P-values for Fig 5F for MCF7-ABCG2 (Table M); P-values for Fig 5F for MDA231-CD44 (Table N); P-values for Fig 5F for MDA231-EGFR (Table O); P-values for Fig 5F for HCT116-CD44 (Table P); P-values for Fig 5F for HCT116-TGFβ (Table Q); P-values for Fig 5F for U2OS-CD44 (Table R); P-values for Fig 5F for U2OS-CD133 (Table S); P-values for Fig 5F for AGS-CD44 (Table T); P-values for Fig 5F for AGS-OCT4 (Table U).
(PDF)

S2 File. Tables of p-values for statistically significant differences for the data with an asterisk in Figs 6 and 7. P-values for Fig 6G (Table A); P-values for Fig 6H (Table B); P-values for Fig 6I (Table C); P-values for Fig 6J (Table D); P-values for Fig 6K (Table E); P-values for Fig 6L (Table F); P-values for Fig 7A (Table G); P-values for Fig 7B (Table H); P-values for Fig 7D (Table I); P-values for Fig 7E (Table J); P-values for Fig 7F (Table K); P-values for Fig 7G (Table L); P-values for Fig 7H (Table M); P-values for Fig 7I (Table N); P-values for Fig 7K (Table O).
(PDF)

Acknowledgments

This work was supported by research grants to E. Jabbari from the National Science Foundation under Award Numbers CBET1403545 and IIP150024. Research reported in this publication was supported by the National Institute of Arthritis and Musculoskeletal and Skin Diseases of the National Institutes of Health under Award Number AR063745. The authors thank Danial Barati for assistance with macromer synthesis and Dr. Seyed Ramin Pajoum Shariati for assistance with cultivation of cancer cells.

Author Contributions

Conceived and designed the experiments: EJ SKS. Performed the experiments: SKS SM LD. Analyzed the data: SKS SM EJ LD. Contributed reagents/materials/analysis tools: EJ SKS SM LD. Wrote the paper: EJ.

References

1. Tobin NP, Harrell JC, Lovrot J, Egyhazi Brage S, Frostvik-Stolt M, Ferno M, et al. (2015) The molecular subtype and tumor characteristics of breast cancer metastases significantly influence patient post-relapse survival. Ann Oncol 26: 81–88. doi: 10.1093/annonc/mdu498 PMID: 25361981
2. Fenner A (2012) Prostate cancer: Hypoxia predicts relapse and recurrence after radiotherapy. Nat Rev Urol 9: 237.
3. Stokes ME, Thompson D, Montoya EL, Weinstein MC, Winer EP, Earle CC (2008) Ten-year survival and cost following breast cancer recurrence: Estimates from seer-medicare data. Value Health 11: 213–20. doi: 10.1111/j.1524-4733.2007.00226.x PMID: 18380633
4. Tsai WS, Hsieh PS, Yeh CY, Chiang JM, Tang R, Chen JS, et al. (2011) Long-term survival benefits of adjuvant chemotherapy by decreasing incidence of tumor recurrence without delaying relapse in stage III colorectal cancer. Int J Colorectal Dis 26: 1329–38. doi: 10.1007/s00384-011-1214-8 PMID: 21556841

5. Pattabiraman DR, Weinberg RA (2014) Tackling the cancer stem cells—what challenges do they pose? Nature Rev Drug Discov 13: 497–512.
6. Liu TJ, Sun BC, Zhao XL, Zhao XM, Sun T, Gu Q, et al. (2013) CD133+ cells with cancer stem cell characteristics associates with vasculogenic mimicry in triple-negative breast cancer. Oncogene 32: 544–53. doi: 10.1038/onc.2012.85 PMID: 22469978
7. Fang Y, Xiang J, Chen Z, Gu X, Li Z, Tang F, et al. (2012) miRNA expression profile of colon cancer stem cells compared to non-stem cells using the SW1116 cell line. Oncol Rep 28: 2115–24. doi: 10.3892/or.2012.2054 PMID: 23007737
8. Fessler E, Dijkgraaf FE, De Sousa EMF, Medema JP (2013) Cancer stem cell dynamics in tumor progression and metastasis: Is the microenvironment to blame? Cancer Lett 341: 97–104. doi: 10.1016/j.canlet.2012.10.015 PMID: 23089245
9. Engler AJ, Sen S, Sweeney HL, Discher DE (2006) Matrix elasticity directs stem cell lineage specification. Cell 126: 677–689. PMID: 16923388
10. Pek YS, Wan ACA, Ying JY (2010) The effect of matrix stiffness on mesenchymal stem cell differentiation in a 3D thixotropic gel. Biomaterials 31: 385–391. doi: 10.1016/j.biomaterials.2009.09.057 PMID: 19811817
11. Paszek MJ, Zahir N, Johnson KR, Lakins JN, Rozenberg GI, Gefen A, et al. (2005) Tensional homeostasis and the malignant phenotype. Cancer Cell 8: 241–54. PMID: 16169468
12. Baker EL, Lu J, Yu DH, Bonnecaze RT, Zaman MH (2010) Cancer cell stiffness: Integrated roles of three-dimensional matrix stiffness and transforming potential. Biophys J 99: 2048–2057. doi: 10.1016/j.bpj.2010.07.051 PMID: 20923638
13. Jamal M, Rath BH, Tsang PS, Camphausen K, Tofilon PJ (2012) The brain microenvironment preferentially enhances the radioresistance of CD133(+) glioblastoma stem-like cells. Neoplasia 14: 150–158. PMID: 22431923
14. Chen L, Xiao Z, Meng Y, Zhao Y, Han J, Su G, et al. (2012) The enhancement of cancer stem cell properties of MCF-7 cells in 3D collagen scaffolds for modeling of cancer and anti-cancer drugs. Biomaterials 33: 1437–1444. doi: 10.1016/j.biomaterials.2011.10.056 PMID: 22078807
15. Hale NA, Yang Y, Rajagopalan P (2010) Cell migration at the interface of a dual chemical-mechanical gradient. ACS Appl Mater Interf 2: 2317–2324.
16. Yang X, Sarvestani SK, Moeinzadeh S, He X, Jabbari E (2013) Three-dimensional-engineered matrix to study cancer stem cells and tumorsphere formation: Effect of matrix modulus. Tissue Eng Part A 19: 669–84. doi: 10.1089/ten.TEA.2012.0333 PMID: 23013450
17. Yang X, Sarvestani SK, Moeinzadeh S, He X, Jabbari E (2013) Effect of CD44 binding peptide conjugated to an engineered inert matrix on maintenance of breast cancer stem cells and tumorsphere formation. PLoS One 8: e59147. doi: 10.1371/journal.pone.0059147 PMID: 23527117
18. Tang X, Kuhlenschmidt TB, Zhou J, Bell P, Wang F, Kuhlenschmidt MS, et al. (2010) Mechanical force affects expression of an in vitro metastasis-like phenotype in HCT-8 cells. Biophys J 99: 2460–2469. doi: 10.1016/j.bpj.2010.08.034 PMID: 20959086
19. Mylona E, Dailiana ZH, Trepat X, Lagoudakis MG (2008) Substrate rigidity dictates phenotype, survival, and mechanics of primary human osteosarcoma cells. Eur Symp Biomed Eng 1–4.
20. He X, Ma J, Jabbari E (2008) Effect of grafting RGD and BMP-2 protein-derived peptides to a hydrogel substrate on osteogenic differentiation of marrow stromal cells. Langmuir 24: 12508–12516. doi: 10.1021/la802447v PMID: 18837524
21. Yu F, Li J, Chen H, Fu J, Ray S, Huang S, et al. (2011) Kruppel-like factor 4 (KLF4) is required for maintenance of breast cancer stem cells and for cell migration and invasion. Oncogene 30: 2161–2172. doi: 10.1038/onc.2010.591 PMID: 21242971
22. Yan J, Sun YH, Zhu H, Marcu L, Revzin A (2009) Enzyme-containing hydrogel micropatterns serving a dual purpose of cell sequestration and metabolite detection. Biosens Bioelectron 24: 2604–2610. doi: 10.1016/j.bios.2009.01.029 PMID: 19251408
23. He X, Yang X, Jabbari E (2012) Combined effect of osteopontin and BMP-2 derived peptides grafted to an adhesive hydrogel on osteogenic and vasculogenic differentiation of marrow stromal cells. Langmuir 28: 5387–5397. doi: 10.1021/la205005h PMID: 22372823
24. Henderson JA, He X, Jabbari E (2008) Concurrent differentiation of marrow stromal cells to osteogenic and vasculogenic lineages. Macromol Biosci 8: 499–507. doi: 10.1002/mabi.200800093 PMID: 17941111
25. Sun YR, Kong WQ, Falk A, Hu J, Zhou LF, Pollard S, et al. (2009) CD133 (prominin) negative human neural stem cells are clonogenic and tripotent. PLoS One 4: e5498. doi: 10.1371/journal.pone.0005498 PMID: 19430532

26. Abu-Ali S, Fotovati A, Shirasuna K (2008) Tyrosine-kinase inhibition results in EGFR clustering at focal adhesions and consequent exocytosis in upar down-regulated cells of head and neck cancers. Mol Cancer 7: 47. doi: 10.1186/1476-4598-7-47 PMID: 18519000

27. Meyer JS, Shearer RL, Capowski EE, Wright LS, Wallace KA, McMillan EL, et al. (2009) Modeling early retinal development with human embryonic and induced pluripotent stem cells. Proc Natl Acad Sci U S A 106: 16698–16703. doi: 10.1073/pnas.0905245106 PMID: 19706890

28. Xie SP, Macedo P, Hew M, Nassenstein C, Lee KY, Chung KF (2009) Expression of transforming growth factor-beta (TGF-beta) in chronic idiopathic cough. Respir Res 10: 40. doi: 10.1186/1465-9921-10-40 PMID: 19463161

29. Livak KJ, Schmittgen TD (2001) Analysis of relative gene expression data using real-time quantitative pcr and the 2(-delta delta c(t)) method. Methods 25: 402–8. PMID: 11846609

30. Lynn AD, Kyriakides TR, Bryant SJ (2010) Characterization of the in vitro macrophage response and in vivo host response to poly(ethylene glycol)-based hydrogels. J Biomed Mater Res Part A 93: 941–953.

31. Benjamini Y, Hochberg Y (1995) Controlling the false discovery rate—a practical and powerful approach to multiple testing. J Royal Stat Soc Ser B Meth 57: 289–300.

32. Britton KM, Eyre R, Harvey IJ, Stemke-Hale K, Browell D, Lennard TW, et al. Breast cancer, side population cells and ABCG2 expression. Cancer Lett 323: 97–105. doi: 10.1016/j.canlet.2012.03.041 PMID: 22521545

33. Hiraga T, Ito S, Nakamura H (2011) Side population in MDA-MB-231 human breast cancer cells exhibits cancer stem cell-like properties without higher bone-metastatic potential. Oncol Rep 25: 289–296. PMID: 21109989

34. Subik K, Lee JF, Baxter L, Strzepek T, Costello D, Crowley P, et al. (2010) The expression patterns of ER, PR, HER2, Ck5/6, EGFR, Ki-67 and AR by immunohistochemical analysis in breast cancer cell lines. Breast Cancer Auckl 4: 35–41. PMID: 20697531

35. Ricardo S, Vieira AF, Gerhard R, Leitao D, Pinto R, Cameselle-Teijeiro JF, et al. (2011) Breast cancer stem cell markers CD44, CD24 and ALDH1: Expression distribution within intrinsic molecular subtype. J Clin Path 64: 937–946. doi: 10.1136/jcp.2011.090456 PMID: 21680574

36. Soofi SS, Last JA, Liliensiek SJ, Nealey PF, Murphy CJ (2009) The elastic modulus of matrigel (TM) as determined by atomic force microscopy. J Struct Biol 167: 216–219. doi: 10.1016/j.jsb.2009.05.005 PMID: 19481153

37. Louie E, Nik S, Chen JS, Schmidt M, Song B, Pacson C, et al. (2010) Identification of a stem-like cell population by exposing metastatic breast cancer cell lines to repetitive cycles of hypoxia and reoxygenation. Breast Cancer Res 12: R94. doi: 10.1186/bcr2773 PMID: 21067584

38. Holliday DL, Speirs V (2011) Choosing the right cell line for breast cancer research. Breast Cancer Res 13: 215. doi: 10.1186/bcr2889 PMID: 21884641

39. Sakai K, Kurokawa T, Furui Y, Kuronuma Y, Sekiguchi M, Ando J, et al. (2011) Invasion of carcinoma cells into reconstituted type I collagen gels: Visual real-time analysis by time-lapse microscopy. Biosci Trends 5: 10–16. PMID: 21422595

40. O'Brien CA, Pollett A, Gallinger S, Dick JE (2007) A human colon cancer cell capable of initiating tumour growth in immunodeficient mice. Nature 445: 106–110. PMID: 17122772

41. Roy S, Majumdar AP (2012) Signaling in colon cancer stem cells. J Mol Signal 7: 11. doi: 10.1186/1750-2187-7-11 PMID: 22866952

42. Chen Z, Xu WR, Qian H, Zhu W, Bu XF, Wang S, et al. (2009) OCT4, a novel marker for human gastric cancer. J Surg Oncol 99: 414–419. doi: 10.1002/jso.21270 PMID: 19347886

43. Tirino V, Desiderio V, Paino F, De Rosa A, Papaccio F, Fazioli F, et al. (2011) Human primary bone sarcomas contain CD133+ cancer stem cells displaying high tumorigenicity in vivo. FASEB J 25: 2022–2030. doi: 10.1096/fj.10-179036 PMID: 21385990

44. Jaggupilli A, Elkord E (2012) Significance of CD44 and CD24 as cancer stem cell markers: An enduring ambiguity. Clin Dev Immunol 708036.

45. Hibino S, Shibuya M, Engbring JA, Mochizuki M, Nomizu M, Kleinman HK (2004) Identification of an active site on the laminin alpha 5 chain globular domain that binds to CD44 and inhibits malignancy. Cancer Res 64: 4810–4816. PMID: 15256450

46. Peppas NA, Barr-Howell BD (1986) Characterization of the cross-linked structure of hydrogels. Hydrogels in Medicine and Pharmacy 1: 27–56.

47. Flecha FLG, Levi V (2003) Determination of the molecular size of bsa by fluorescence anisotropy. Biochem Mol Biol Ed 31: 319–322.

48. Engberg K, Frank CW (2011) Protein diffusion in photopolymerized poly(ethylene glycol) hydrogel networks. Biomed Mater 6: 055006. doi: 10.1088/1748-6041/6/5/055006 PMID: 21873762

49. Scheel C, Eaton EN, Li SH, Chaffer CL, Reinhardt F, Kah KJ, et al. (2011) Paracrine and autocrine signals induce and maintain mesenchymal and stem cell states in the breast. Cell 145: 926–40. doi: 10.1016/j.cell.2011.04.029 PMID: 21663795

50. Yamamoto M, Taguchi Y, Ito-Kureha T, Semba K, Yamaguchi N, Inoue J (2013) NF-kb non-cell-autonomously regulates cancer stem cell populations in the basal-like breast cancer subtype. Nature Commun 4: 2299.

51. Lu J, Ye XC, Fan F, Xia L, Bhattacharya R, Bellister S, et al. (2013) Endothelial cells promote the colorectal cancer stem cell phenotype through a soluble form of jagged-1. Cancer Cell 23: 171–185. doi: 10.1016/j.ccr.2012.12.021 PMID: 23375636

52. Fillmore CM, Gupta PB, Rudnick JA, Caballero S, Keller PJ, Lander ES, et al. (2010) Estrogen expands breast cancer stem-like cells through paracrine FGF/TBX3 signaling. Proc Natl Acad Sci U S A 107: 21737–21742. doi: 10.1073/pnas.1007863107 PMID: 21098263

53. Tse HTK, Weaver WM, Di Carlo D (2012) Increased asymmetric and multi-daughter cell division in mechanically confined microenvironments. PLoS One 7: e38986. doi: 10.1371/journal.pone.0038986 PMID: 22761717

54. Medema JP (2013) Cancer stem cells: The challenges ahead. Nature Cell Biol 15: 338–344. doi: 10.1038/ncb2717 PMID: 23548926

55. Boyd NF, Li Q, Melnichouk O, Huszti E, Martin LJ, Gunasekara A, et al. (2014) Evidence that breast tissue stiffness is associated with risk of breast cancer. PLoS One 9: e100937. doi: 10.1371/journal.pone.0100937 PMID: 25010427

56. Tilghman RW, Cowan CR, Mih JD, Koryakina Y, Gioeli D, Slack-Davis JK, et al. (2010) Matrix rigidity regulates cancer cell growth and cellular phenotype. PLoS One 5: e12905. doi: 10.1371/journal.pone.0012905 PMID: 20886123

57. Biddle A, Mackenzie IC (2012) Cancer stem cells and emt in carcinoma. Cancer Metastasis Rev 31: 285–293.

58. Mani SA, Guo W, Liao MJ, Eaton EN, Ayyanan A, Zhou AY, et al. (2008) The epithelial-mesenchymal transition generates cells with properties of stem cells. Cell 133: 704–715. doi: 10.1016/j.cell.2008.03.027 PMID: 18485877

59. Zeisberg M, Neilson EG (2009) Biomarkers for epithelial-mesenchymal transitions. J Clin Invest 119: 1429. doi: 10.1172/JCI36183 PMID: 19487819

60. Lamouille S, Xu J, Derynck R (2014) Molecular mechanisms of epithelial-mesenchymal transition. Nature Rev Mol Cell Biol 15: 178–196.

61. Kalluri R, Weinberg RA (2009) The basics of epithelial-mesenchymal transition. J Clin Invest 119: 1420–1428. doi: 10.1172/JCI39104 PMID: 19487818

62. Cordenonsi M, Zanconato F, Azzolin L, Forcato M, Rosato A, Frasson C, et al. (2011) The Hippo transducer TAZ confers cancer stem cell-related traits on breast cancer cells. Cell 147: 759–772. doi: 10.1016/j.cell.2011.09.048 PMID: 22078877

63. Dupont S, Morsut L, Aragona M, Enzo E, Giulitti S, Cordenonsi M, et al. (2011) Role of YAP/TAZ in mechanotransduction. Nature 474: 179–U212. doi: 10.1038/nature10137 PMID: 21654799

64. Staubach S, Hanisch FG (2011) Lipid rafts: Signaling and sorting platforms of cells and their roles in cancer. Expert Rev Proteomics 8: 263–277. doi: 10.1586/epr.11.2 PMID: 21501018

65. Ferraro JT, Daneshmand M, Bizios R, Rizzo V (2004) Depletion of plasma membrane cholesterol dampens hydrostatic pressure and shear stress-induced mechanotransduction pathways in osteoblast cultures. Am J Physiol Cell Physiol 286: C831–C839. PMID: 14644772

66. Ye J, Wu D, Wu P, Chen ZG, Huang J (2014) The cancer stem cell niche: Cross talk between cancer stem cells and their microenvironment. Tumor Biol 35: 3945–3951